

Development of a fast neutron spectrometer based on a plastic fiber array

Fan-Jian Zeng^{1,2,3} · Li-Yang Sun^{1,2,3} · Kai Zhuang^{1,2} · Heng An⁴ ·
Yu-Xiong Xue⁴ · Xiao-Ming Wang^{1,2} · Dao-Wu Li^{1,2} · Zhi-Ming Zhang^{1,2} ·
Bao-Tong Feng^{1,2} · Pei-Lin Wang^{1,2} · Jia-Le Cai^{1,2,3} · Xiu-Bo Qin^{1,2} · De-Tian Li⁴

Received: 8 February 2017 / Revised: 19 April 2017 / Accepted: 2 May 2017 / Published online: 16 June 2017

© Institute of High Energy Physics, Chinese Academy of Sciences; China Nuclear Electronics and Nuclear Detection Society and Springer Science+Business Media Singapore 2017

Abstract

Objective A three-dimensional position-sensitive fast neutron spectrometer is designed to measure fast neutron spectrum over 10 MeV.

Methods The detector consists of a 16×16 mutually perpendicular plastic scintillation fiber array coupled to 2×2 Hamamatsu H8500C position-sensitive photomultiplier tubes by optical fibers. The fiber array is fabricated with $0.5 \text{ mm} \times 3 \text{ mm}$ fibers and 3-mm square fibers.

Results Due to the combined application of different sizes of fibers, the detector can broaden energy dynamic range and meanwhile have good detection efficiency. The method of the combined application of different sizes of plastic fibers in the array may provide a solution to measure wider energy range of solar neutrons.

Conclusion In this paper, we used FLUKA to simulate the performance of the detector model and report the results of experimental studies with neutrons from a pulsed D-T neutron.

Keywords Fast neutron · Different sizes · Fiber array · Energy range

Introduction

Recently, requirements for precise measurement of fast neutrons combined with energy spectroscopy are increasing rapidly, ranging from neutron radiotherapy, the space environment monitoring, and regulation of nuclear materials. However, classic fast neutron detectors often work at low energy range below several MeV, and most of the classic detector can hardly measure the energy, the direction, and the emission time of the original neutrons. So, new methods must be used to get above-mentioned information of neutrons [1–10].

Over the past decade, a plastic scintillation fiber array model has been developed for fast neutron detection, utilizing the mechanism of one or double neutron–proton scattering to measure the direction or energy of the incident neutron. Based on this model, the SONTRAC detector with a bundle of 0.25 mm fibers is developed by Ryan et al. [11–15] to measure the energy and direction of neutrons at the energy range of 20–250 MeV. Due to the small size of the fiber used, the detector actually has the potential to detect lower energy neutrons according to our simulation in “Simulation methods and results” section. The fiber array is read out by CCD cameras and photomultiplier tubes. Based on this designing scheme, the detector has good position and energy resolution, not sacrificing detection efficiency. However, the trigger rate is lower than 20 Hz as CCDs work slowly, so that the detector is difficult to measure in real neutron environment.

Afterward, a fast neutron imaging telescope (FNIT) [16–18] is developed to monitor special nuclear material (SNM). In this detector, the recoil proton is seen to lose all its energy at a point. So the detection energy range is below 20 MeV.

In addition, on July 16, 2009, a new solar neutron telescope [19, 20] was launched on the Space Shuttle Endeavour

✉ Xiu-Bo Qin
qinxb@ihep.ac.cn

¹ Institute of High Energy Physics, Chinese Academy of Sciences, Beijing 100049, China

² Beijing Engineering Research Center of Radiographic Techniques and Equipment, Beijing 100049, China

³ University of Chinese Academy of Sciences, Beijing 100049, China

⁴ Lanzhou Institute of Physics, Chinese Academy of Space Technology, Lanzhou, Gansu 730000, China

with the aim of measuring 20–120 MeV fast neutrons at the International Space Station (ISS). The detector has good detection efficiency and high trigger rate for fast neutrons. However, the detector cannot measure neutrons below 35 MeV as the size of the plastic scintillation fiber used in the detector is as large as 3 mm.

To improve the detection limit in low energy, the fiber size in the plastic fiber array should be smaller. However, due to the limit of the electronic scale, the volume of the detector is small, so the detection efficiency and the upper energy limit are sacrificed. On the other hand, to improve the detection efficiency and the upper energy detection limit, the fiber size should be large. Then the detector cannot detect relatively lower energy neutrons.

In our paper, we provide a method to achieve larger energy range, which may be used to measure the wider energy spectrum of the solar neutrons. A three-dimensional position-sensitive scintillation detector combined with 0.5 mm square fibers and 3 mm square fibers is designed to measure fast neutron spectrum over 10 MeV. Due the combined application of two sizes of fibers, the detector can broaden the energy range, without increasing electronic channels.

Materials and methods

Neutron–proton elastic scattering principle

As neutrons are electrically neutral, they must be detected by indirect ways. The method of detecting neutrons usually begins while neutrons are interacting with a nucleus. Through the reaction, one or more secondary charged particles are emitted. By means of detecting the electrical signal produced by the secondary particles, neutrons can be measured indirectly. The plastic scintillator is an ideal material to detect fast neutrons as it is cheap, flexible, and full of hydrogen, which has a large cross section. Moreover, the recoil proton in high energy transfers a long path, which could be measured possibly.

The main interaction of fast neutrons in plastic scintillation is neutron–proton (n–p) elastic scattering reaction and neutron–carbon (n–C) reaction. The n–p elastic scattering events are most effective to reconstruct information of the recoil neutrons with conservation of energy and momentum. As is shown in Fig. 1, the recoil proton can be measured in the detector.

If the direction of the incident neutron is known, we can calculate the energy of the original neutron by the formula below:

$$E_n = E_p / \cos^2 \theta \quad (1)$$

where E_n and E_p are the kinetic energy of the incident neutron and the kinetic energy of the recoil proton, respectively.

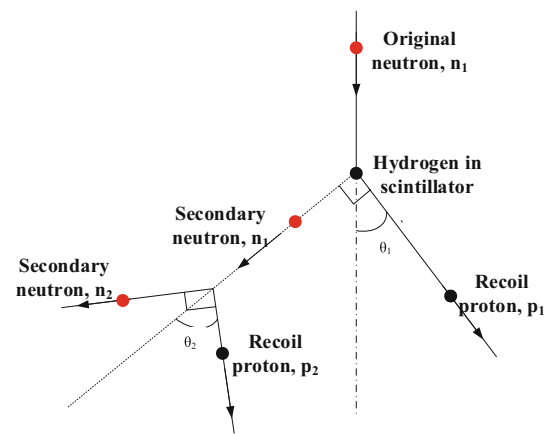


Fig. 1 Mechanism of n–p elastic scattering, the tracks of recoil protons are visible

The secondary neutron and the recoil proton move perpendicularly to each other.

If the energy of the incident neutron is known, the direction of the original neutron can be calculated in the same way by the formula below:

$$\theta = \pm \cos^{-1} \sqrt{\frac{E_p}{E_n}} \quad (2)$$

If both the direction and the energy of the incident neutron are unknown, double n–p elastic scattering rather than one n–p elastic scattering is effective for the event reconstruction.

In our detector model, the neutrons travel vertically into the surface of the detector, so the energy of the incident neutrons can be calculated by one n–p interaction.

Detector design

For a certain recoil proton, its track length is measured by counting number of the fibers which it passes through. To obtain high accuracy measurement of recoil proton track, the fiber size should be small. However, smaller fiber size will certainly lead to more signal output, which means a large scale of the electronic channels. Taking into account the energy range, detection efficiency, and electronic channels, two different sizes of plastic scintillation fibers are used to fabricate the fiber array.

As is shown in Fig. 2, the 3D neutron detector consists of 16 orthogonal layers, and each layer contains 16 sticks of scintillation fibers. The above four layers include 64 pieces of 0.5 mm × 3 mm fibers, as every fiber consists of six 0.5 mm square fibers to detect the relatively low-energy neutrons above 10 MeV. In addition, the bottom 12 layers include 192 pieces of 3 mm square fibers to detect the relatively higher energy neutrons above 30 MeV. Finally, both ends of

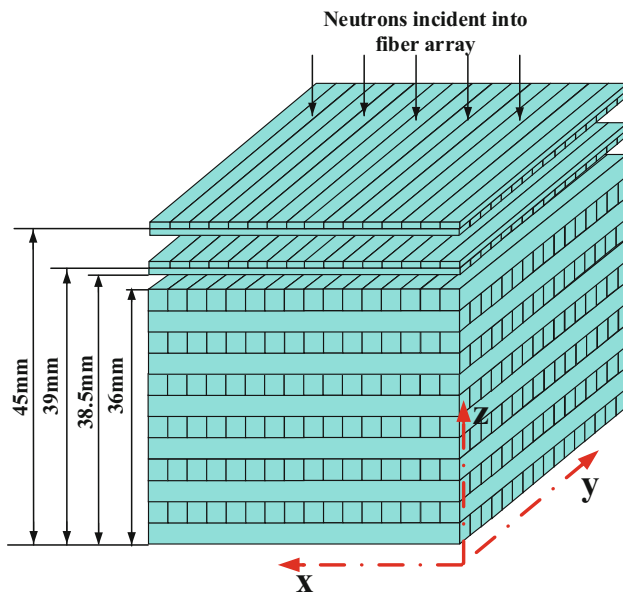


Fig. 2 Plastic fiber array model is fabricated with $(0.5 \times 3 \times 48)$ and $(0.5 \times 3 \times 48)$ mm³ plastic scintillation fiber sticks

each fiber are coupled to an anode of a Hamamatsu H8500C position-sensitive photomultiplier tube (PSPMT).

The square plastic scintillation fibers used are Saint-Gobain BCF-10, which has good properties of fast decay time and high light yield. To ensure a wide energy range, two different fiber sizes are selected without sacrificing detection efficiency. One is 0.5 mm square fibers for the top four layers and the other is 3 mm square fiber for the bottom twelve layers. The core of BCF-10 is made of polystyrene. The cladding layer of square BCF-10 fiber is polymethyl methacrylate (PMMA) and the thickness of the fiber is 4% of the fiber size. The peak of wavelength from BCF-10 fiber is 432 nm, which is well matched to the photocathode efficiency curve of the Hamamatsu H8500C PSPMT. Moreover, due to the reduction of power consumption, volume, and weight of the detector, we choose this type of PMT.

Signal processing flow

The data acquisition process is shown in Fig. 3. The incident neutron firstly produces a proton, which deposits energy along its track in the plastic fiber array and creates fluorescence immediately. Afterward, the scintillation fluorescence is transmitted to four H8500C PSPMTs by optical fibers. Then, current signals are generated in the multi-anodes of the H8500C PSPMTs.

Next, 256 current signals in total from the four PSPMTs are processed in the amplifier and shaper boards. Each current signal is converted and amplified to enough voltage and then shaped to be approximately Gaussian. Meanwhile, the 12th staged dynode signal of each PSPMT is fed into a comparator

circuit, then fed into an OR logical circuit to be trigger signal. The output of an amplified and shaped signal and the trigger signal is shown in Fig. 4.

Furthermore, the 256 analog signals are transformed to digital signals in ADCs. Then position and energy information of each event will be calculated in FPGA. Finally, data of each event will be packed and transmitted by kilo mega network to PC to reconstruct the energy of the original neutrons.

Gain consistency calibration of the system

H8500C PSPMTs have a non-uniform anode gain, which can degrade the intrinsic performance of the detector module. In particular, the gain uniformity distorts the signal amplitude linearity of each element, so as to seriously affect the energy spectrum measurement. So we need necessarily calibrate the gain of each anode the same.

The aim of this section is to develop a gain compensation method for the H8500C and evaluate the resulting enhancement in the performance of the detector. Measurements are taken by coupling the same LYSO crystal to the center of each anode, respectively. The crystal is covered with high-reflected film and a 1 μ Ci ¹³⁷Cs point source with a nominal size 0.5 mm is utilized in the measurements. The H8500C PMTs used in the detector work at the same voltage -700 V, supplied by a stabilized high voltage power source and the measurements are taken under strict darkroom conditions. For anode uniformity measurements, each detection element spectrum is read out, respectively. Then, the gain of each anode of the H8500C is normalized with respect to the maximum peak channel value obtained. Finally, the gain uniformity of all elements is adjusted to be within 4%.

Simulation methods and results

The simulation is carried out using FLUKA, a toolkit package developed at INFN and CERN, to simulate the performance of the detector. The toolkit is made up of FLUKA core code and FLUKA user routines, and it is best known for its capacity to handle transport and interactions of hadrons, heavy ions, and electromagnetic particles in any material for a wide energy range from thermal neutrons to cosmic rays [21].

In this simulation work, the physical data model is chosen as a precision model, which can depict transport and interactions of neutrons below 20 MeV. For neutrons with energy over 20 MeV, a pointwise transport method is adopted to describe the elastic scattering or inelastic scattering process of neutron–hydrogen reaction and neutron–carbon reaction and depict the transport of secondary particles such as protons. For neutrons with energy lower than 20 MeV, multi-group scattering model [22] is used to depict the transport of

2.3 Signal processing flow

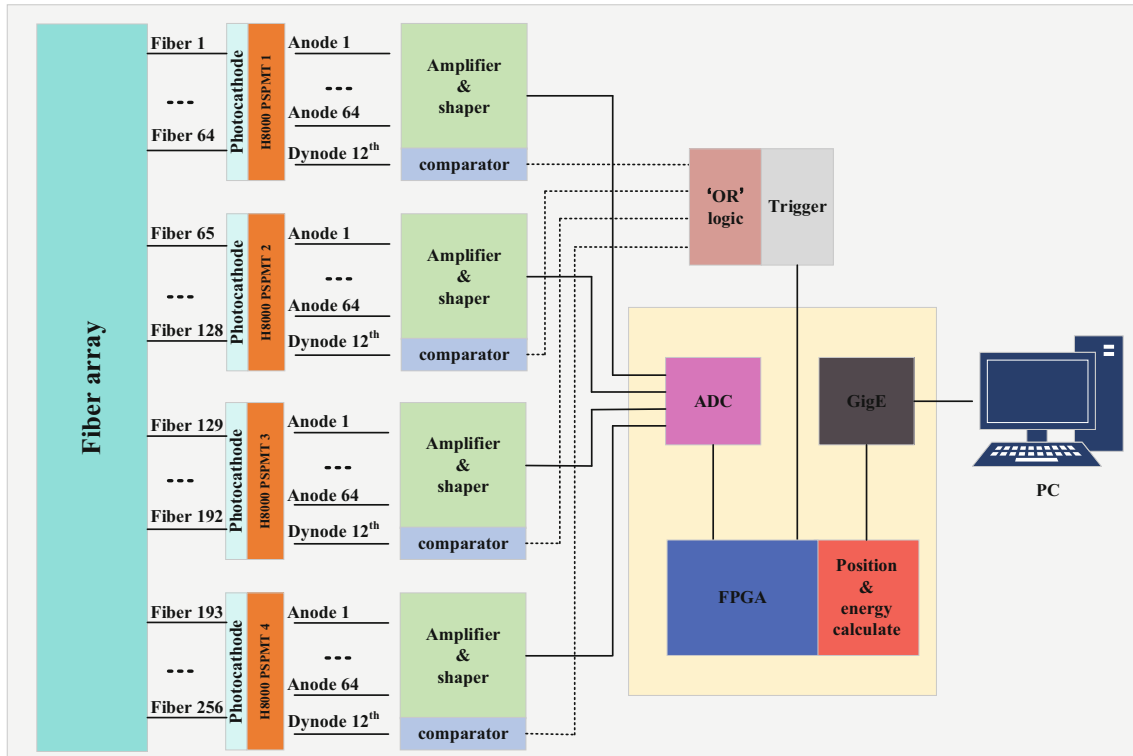


Fig. 3 Data acquisition flow chart

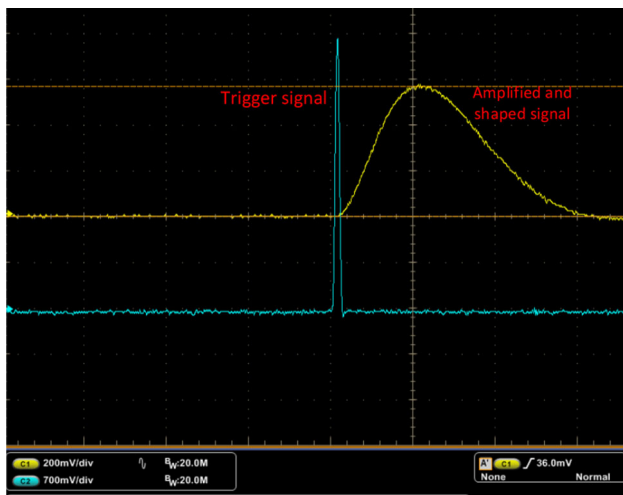


Fig. 4 One of the 256 analog signals and the trigger signal. The width of the analog outputs is 1.2 μ s. The width of the trigger signal is 40 ns

neutrons by splitting the neutron energy into multiple intervals and setting the average cross section of each interval as reaction cross section. In addition, we utilize the user-defined FLUKA user routines to label the recoil protons based on types of neutrons and hydrogens nuclear interaction.

As is shown in Fig. 4. The recoil protons pass through almost along straight lines, and the penetration depth of the

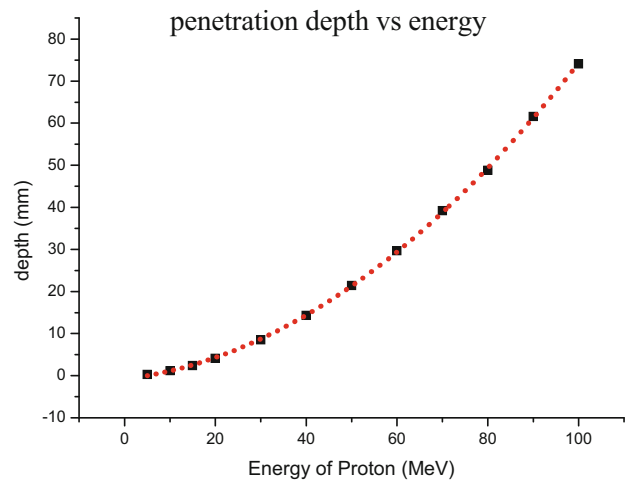


Fig. 5 Penetration depth of recoil protons with different energies

protons grows exponentially with energy, which means the recoil proton deposits more and more energy per length along its track. Figure 5 shows recoil protons with certain energy track almost a certain depth. The proton at 10 MeV can go about 1 mm, which is two times the thickness of the 0.5 mm square fiber. So, we can estimate the lowest energy limit of the fiber array model is about 10 Mev as is shown in Fig. 6. The performance of the fiber array at 14.1 MeV is simulated

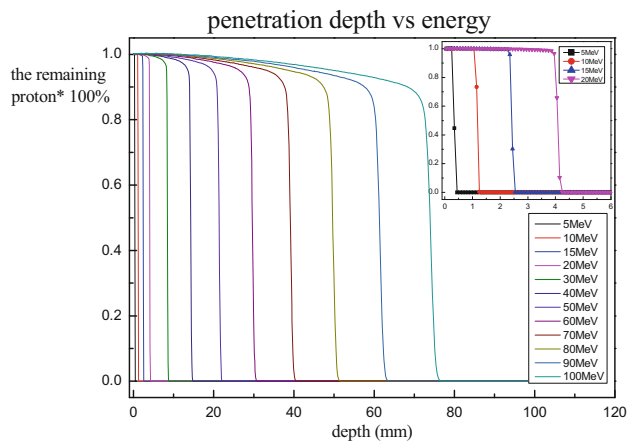


Fig. 6 Remaining protons at certain energies with different depths

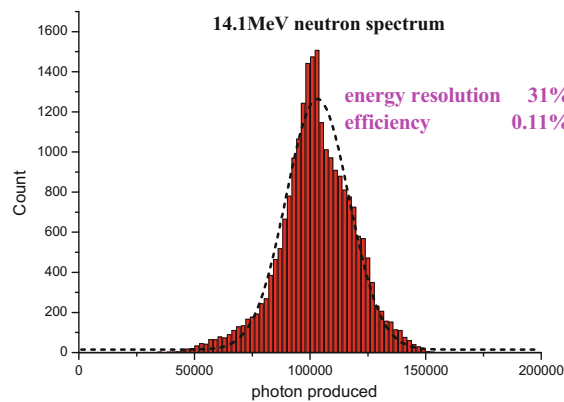


Fig. 7 Spectrum of neutrons at 14.1 MeV by the fiber array model

as is shown in Fig. 7. The energy resolution is 31% and the detection efficiency is 0.11%.

The energy resolution and efficiency of the fiber array at other energy are also simulated. As is shown in Figs. 8 and 9, the average energy resolution of the fiber array is about 30%. The detection efficiency is highest at 50 MeV, up to about 0.68%.

Experimental results

Figure 10 illustrates the experimental setup of the measurement in Institute of High Energy Physics (IHEP). The neutrons are generated from an NG-9 pulsed 14.1 MeV D–T neutron source. The generator is set to a total neutron flux of 1.0×10^7 neutrons/s. The detector is placed about 1.6 m from the generator to provide approximately unidirectional neutrons perpendicular to the detector.

The key point of the data processing in the experiment is to select events that can measure the direction of the recoil protons Firstly. In fact, only the 0.5 mm fibers can play a role at 14.1 MeV. As is shown in Fig. 11, to measure the direction

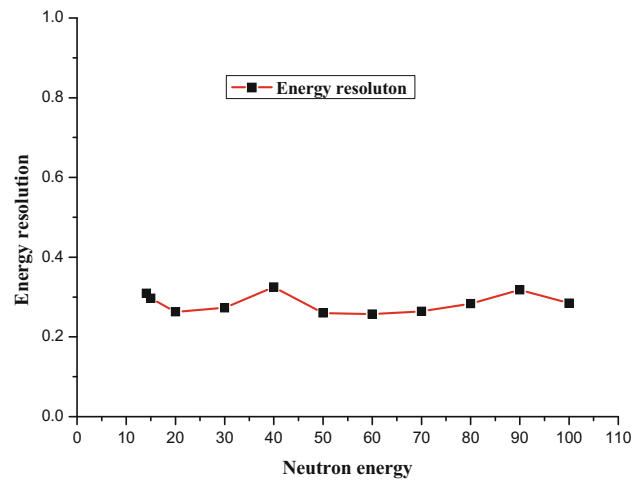


Fig. 8 Energy resolution of neutrons with different energies by the fiber array model

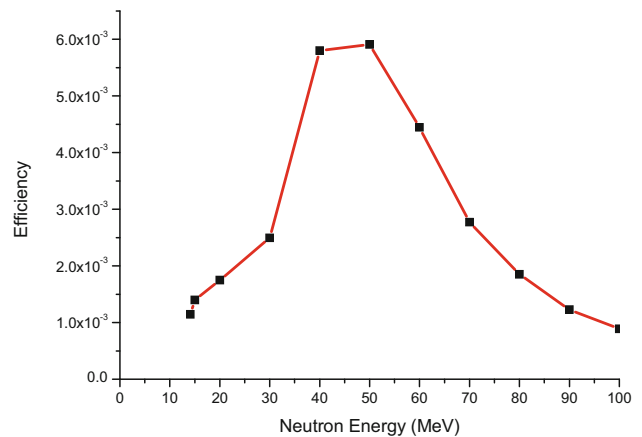
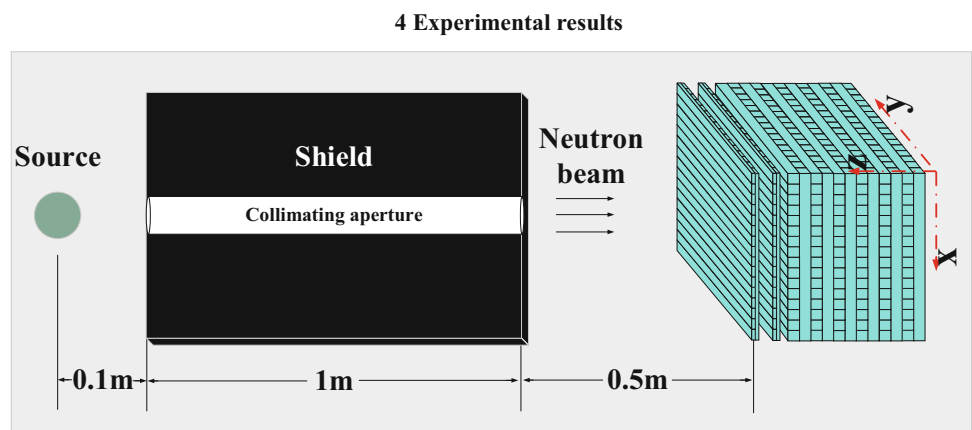


Fig. 9 Detection efficiency of neutrons with different energies by the fiber array model

of a recoil proton, four adjacent layers must be hit. In addition, a threshold is set to discriminate electrons produced by γ rays from recoil protons. Afterward, the effective events must accord with conditions as follows:

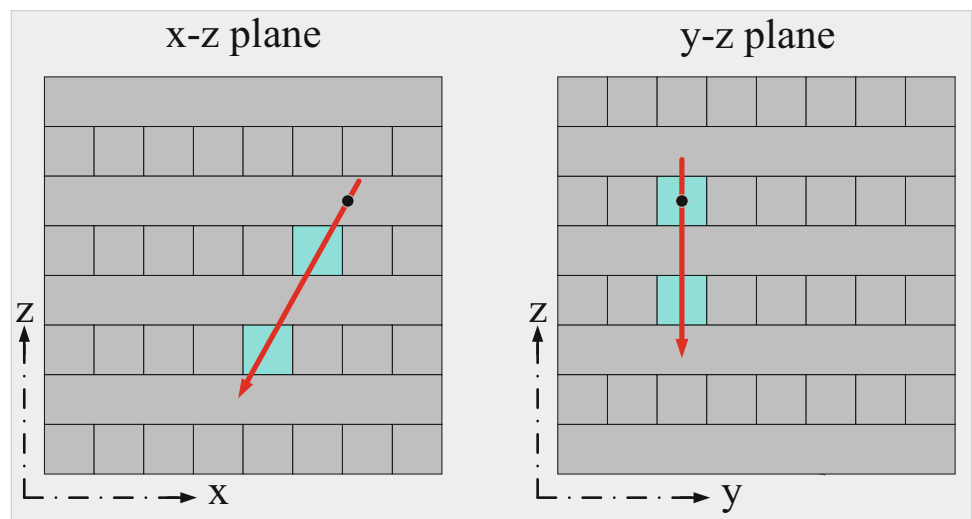
- (a) To measure the direction of the recoil protons, two x -axis coordinates and two y -axis coordinates at least must be known. Therefore, we selected events tracking through at least four layers.
- (b) The layers hit by particles must be continuous and the fibers hit at the same layer must be continuous, so as to make sure it's a single particle event.
- (c) The fiber hit is not at the edge of the fiber array to ensure the recoil proton depositing all energy in the fiber array.
- (d) A discrimination method which allows the rejection of neutron-induced events against γ -ray-induced events was developed by utilizing the different energy track than between protons and electrons in the plastic scintillation.

Fig. 10 Schematic diagram of experimental setup



4 Experimental results

Fig. 11 Schematic diagram of a recoil proton passes through the x - z plane and the y - z plane in the fiber array. To measure the directions in both planes, four adjacent layers must be hit



A proton can generate much more photons than an electron that passes through the same track. Moreover, recoil protons and electrons lose much more energy near the end of their tracks. At 14.1 MeV, energy in one fiber at least is larger than 2 MeV for 0.5 mm fibers.

Figure 12 shows the track of a recoil proton according to the filtering conditions.

For the x - z plane:

$$\tan \theta_x = \frac{\Delta x}{\Delta z} \tag{3}$$

For the y - z plane:

$$\tan \theta_y = \frac{\Delta y}{\Delta z} \tag{4}$$

Then, the direction of the recoil proton, θ is measured from the directions in both x - z plane and y - z plane by formula below:

$$\cos \theta = \frac{\Delta z}{\sqrt{\Delta x^2 + \Delta y^2 + \Delta z^2}} = \frac{1}{1 + \tan^2 \theta_x + \tan^2 \theta_y} \tag{5}$$

The proton energy E_p is reconstructed from energy deposited in the fibers hit. Finally, the incident neutron energy is reconstructed by formula (2). The detector was measured continuously for about 2 h and 15 min under the DT neutron source, with a total of 5.8×10^6 neutrons entering the detector. The final number of neutrons that could be used to reconstruct the incident neutron energy was 5624. Figure 13 shows the neutron spectrum measured at 14.1 MeV.

Discussion

The combined application of 0.5 mm fibers and 3 mm fibers contributes to measuring neutron spectrum over 10 MeV. The important properties of the detector are: wide energy range and good rejection of γ ray events. The energy resolution is 26–32% in the energy range of 14.1–100 MeV in the FLUKA simulation. At 14.1 MeV, the observed energy resolution (43%) in the experiment is worse than that (31%)

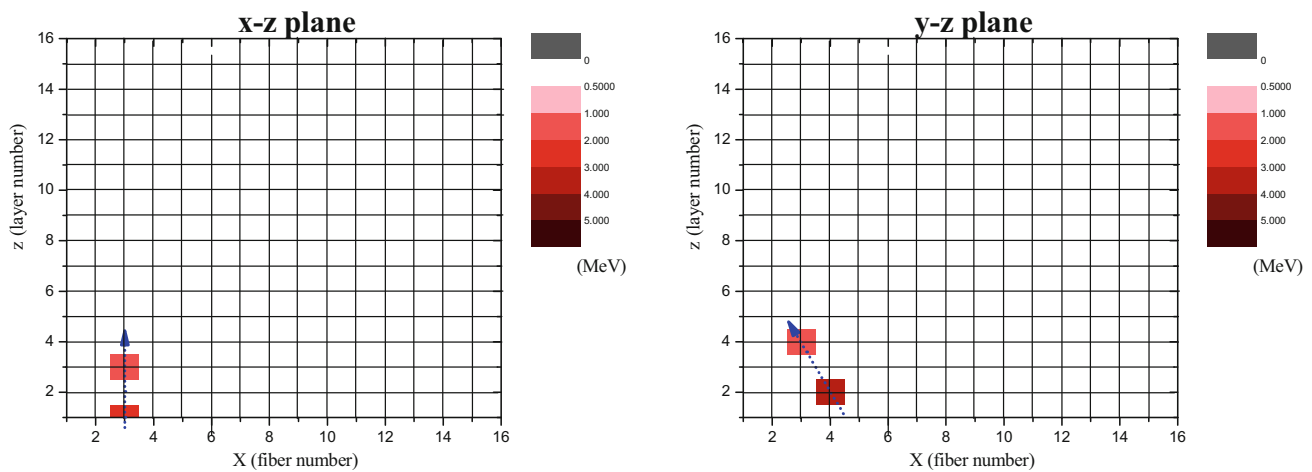


Fig. 12 A recoil proton passes through continuous four 0.5 mm fiber layers. Directions in both the x - z plane and the y - z plane can be measured

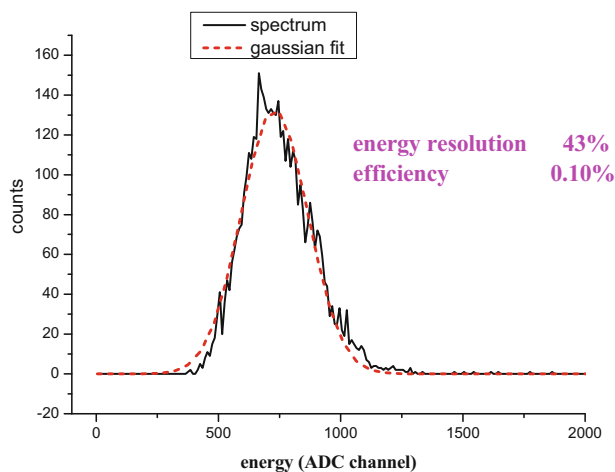


Fig. 13 Neutron spectrum at 14.1 MeV in the experiment

in FLUKA simulation. This may be due to lower statistics in the data counts (~ 2400) than in the FLUKA simulation ($\sim 23,000$). Another source of energy resolution worsening could be electronic noise which is not considered in FLUKA simulation. Moreover, the detection efficiency is about 0.10% in the experiment which accords well with the simulation result (0.11%).

Conclusion

We have demonstrated that a three-dimensional fiber array combined with two sizes of fibers can broaden energy range of neutron detection, without sacrificing efficiency or increasing electronic scale. The methods of using more different sizes of fibers to fabricate the fiber array may broaden the energy range further. The incident neutron energy is

reconstructed by one n-p event. Two n-p events are not taken into account at present.

Moreover, the detector requires further development. Firstly, each scintillation fiber in the detector is coupled to one pixel of PSPMTs by optical fibers. Furthermore, the detector we fabricate has a total of 256 analog signals, which have a large scale. Therefore, we are planning to adopt multiplexers to decrease the digital electronics system in future.

This work constitutes the foundation for our further research in fast neutron detection.

Acknowledgements The author would like to thank An Guang-peng, Yu Bo-Xiang, members of Institute of High Energy Physics (IHEP) for their providing D-T neutron generator.

References

1. R.P. Kelley, J.M. Lewis et al., Measurement of the fast neutron response for 4 He scintillation detectors using a coincidence scattering method. *IEEE Trans. Nucl. Sci.* **63**, 1600–1607 (2016). doi:[10.1109/TNS.2016.2521699](https://doi.org/10.1109/TNS.2016.2521699)
2. S.V. Kurudirek, N.E. Hertel et al., Development of ZnO nanorod-based scintillators grown under a low-temperature hydrothermal method for use in alpha-particle and thermal neutron detectors. *IEEE Trans. Nucl. Sci.* (2016). doi:[10.1109/TNS.2016.2623648](https://doi.org/10.1109/TNS.2016.2623648)
3. M.J. Joyce et al., Real-time, fast neutron coincidence assay of plutonium with a 4-channel multiplexed analyzer and organic scintillators. *IEEE Trans. Nucl. Sci.* **61**, 1340–1348 (2014). doi:[10.1109/TNS.2014.2313574](https://doi.org/10.1109/TNS.2014.2313574)
4. A.Q. Hu, M. Yu et al., Bilateral PIN diode for fast neutron dose measurement. *IEEE Trans. Nucl. Sci.* **61**, 1311–1315 (2014). doi:[10.1109/TNS.2014.2317757](https://doi.org/10.1109/TNS.2014.2317757)
5. J. Glodo, U. Shirwadkar et al., Fast neutron detection with Cs₂LiYCl₆. *IEEE Trans. Nucl. Sci.* **60**, 864–870 (2013). doi:[10.1109/TNS.2012.2227499](https://doi.org/10.1109/TNS.2012.2227499)
6. C. Whitney, E. Johnson et al., DPA-based fast neutron dosimeter for the space environment. *IEEE Trans. Nucl. Sci.* **60**, 830–836 (2013). doi:[10.1109/TNS.2013.2248379](https://doi.org/10.1109/TNS.2013.2248379)
7. F. Berthet, Y. Guhel et al., Influence of thermal and fast neutron irradiation on DC electrical performances of AlGaN/GaN transis-

- tors. *IEEE Trans. Nucl. Sci.* **59**, 2556–2561 (2012). doi:[10.1109/TNS.2012.2209894](https://doi.org/10.1109/TNS.2012.2209894)
8. C. Roecker, A. Bernstein et al., Design of a transportable high efficiency fast neutron spectrometer. *Nucl. Instrum. Methods A* **826**, 21–30 (2016). doi:[10.1016/j.nima.2016.04.032](https://doi.org/10.1016/j.nima.2016.04.032)
 9. A. Giaz, N. Blasi, Fast neutron measurements with 7 Li and 6 Li enriched CLYC scintillators. *Nucl. Instrum. Methods A* **825**, 51–61 (2016). doi:[10.1016/j.nima.2016.03.090](https://doi.org/10.1016/j.nima.2016.03.090)
 10. M.J. Joyce, S. Agar et al., Fast neutron tomography with real-time pulse-shape discrimination in organic scintillation detectors. *Nucl. Instrum. Methods A* **834**, 36–45 (2016). doi:[10.1016/j.nima.2016.07.044](https://doi.org/10.1016/j.nima.2016.07.044)
 11. J.M. Ryan, C.M. Castaneda et al., Design optimization. A scintillating plastic fiber tracking detector for neutron and proton imaging and spectroscopy. *Nucl. Instrum. Methods A* **496**, 228–232 (2003). doi:[10.1016/S0168-9002\(98\)01061-4](https://doi.org/10.1016/S0168-9002(98)01061-4)
 12. J.M. Ryan, J.R. Macri et al., A prototype for SONTRAC, a scintillating plastic fiber tracking detector for neutron imaging and spectroscopy. *IEEE Trans. Nucl. Sci.* (1997). doi:[10.1109/NSSMIC.1997.672725](https://doi.org/10.1109/NSSMIC.1997.672725)
 13. U. Bravar, E.O. Flückiger et al., Atmospheric neutron measurements with the SONTRAC science model, in *IEEE Nuclear Science Symposium Conference Record* (2005). doi:[10.1109/NSSMIC.2005.1596340](https://doi.org/10.1109/NSSMIC.2005.1596340)
 14. P.-T. Bundesanstalt et al., Calculation of fast neutron dose in plastic-coated optical fibres. *IEEE Trans. Nucl. Sci.* **45**, 1570–1575 (1998). doi:[10.1109/23.685241](https://doi.org/10.1109/23.685241)
 15. R.S. Millera, J.R. Macri et al., SONTRAC: an imaging spectrometer for MeV neutrons. *Nucl. Instrum. Methods A* **505**, 36–40 (2003). doi:[10.1016/S0168-9002\(03\)01015-5](https://doi.org/10.1016/S0168-9002(03)01015-5)
 16. B. Pirard, R.S. Woolf et al., Test and simulation of a fast neutron imaging telescope. *Nucl. Instrum. Methods A* **603**, 406–414 (2009). doi:[10.1016/j.nima.2009.02.012](https://doi.org/10.1016/j.nima.2009.02.012)
 17. U. Bravar, J. Paul et al., Development of the fast neutron imaging telescope, in *IEEE Nuclear Science Symposium Conference Record* (2005). doi:[10.1109/NSSMIC.2005.1596217](https://doi.org/10.1109/NSSMIC.2005.1596217)
 18. U. Bravar, J. Paul et al., Design and testing of a position-sensitive plastic scintillator detector for fast neutron imaging. *IEEE Trans. Nucl. Sci.* **53**, 3894–3903 (2006). doi:[10.1109/TNS.2006.886046](https://doi.org/10.1109/TNS.2006.886046)
 19. Y. Muraki, K. Koga et al., Measurement by FIB on the ISS: two emissions of solar neutrons detected? *Adv. Astron.* (2012). doi:[10.1155/2012/379304](https://doi.org/10.1155/2012/379304)
 20. K. Koga, T. Goka et al., Measurement of high-energy neutrons at ISS by SEDA-AP. *Astrophys. Space Sci. Trans.* **2011**(7), 411–416 (2011). doi:[10.5194/astra-7-411-2011](https://doi.org/10.5194/astra-7-411-2011)
 21. G. Battistoni, S. Muraro et al., The FLUKA code: description and benchmarking. *IEEE Trans. Nucl. Sci.* **56**, 2947–2954 (2009). doi:[10.1109/TNS.2009.2028025](https://doi.org/10.1109/TNS.2009.2028025)
 22. A. Ferrari, P.R. Sala, A. Fass'ò, J. Ranft, FLUKA: a multi-particle transport code (Program version 2005), in *CERN-2005-10, INFN/TC-05/11, SLAC-R-773* (CERN, Geneva, 2005)